Experiments in Fluids 3, 261–269 (1985)

Experiments in Fluids

Schlieren interferometry applied to a gravity wave in a density-stratified liquid

F. Peters

Lehrstuhl für Strömungslehre, Universität Essen, D-4300 Essen, FRG

Abstract. A stably density-stratified liquid is produced in a rectangular glass tank by variation of the concentration of salt in water as a function of height. The glass tank is placed into the parallel beam of a schlieren interferometer with Wollaston prism adjusted to produce straight vertical fringes. A gravity wave of the cross wave type is excited and the resulting periodically deforming fringes are recorded by taking photographs. A method is developed to obtain from the fringe patterns results about propagation of the wave in space and time and about amplitude attenuation. The results are compared with the linear theory of Thomas and Stevenson (1972) and excellent agreement is found within the limits of the linear approach.

List of symbols

a	amplitude factor
A	amplitude of body
b	image distance
C, S	functions of η
d	distance of interfering rays
E	envelope of fringes
f	focal length
$\boldsymbol{g}$	gravitational constant
g	object distance
k	integration variable
K	constant
l	tank width
L	characteristic length, Eq. (6)
M	magnification factor
n	refractive index
Re	Reynolds number
s	fringe width
Δs	fringe displacement
t	time
$\dot{V}$	volume flux
w	distance between Wollaston prism and focal point
x_s	distance between $x=0$ and body
x, y, z	coordinates
β	prism constant
ε	small parameter, Eq. (4)
η	similarity coordinate
θ	angle
λ	wavelength of lightsource
ν^*	kinematic viscosity at $y_0=0$
ξ	fluid displacement in x-direction
ϱ	density
ϕ	amplitude function
ω	excitation frequency

Subscripts

0	static values
s	salt
w	water

1 Introduction

A light beam passing through a clear fluid of non-uniform distribution of refractive index is deflected and shifted in phase. Shadowgraph and schlieren methods are sensitive to the deflection. They produce images of varying illumination visualizing changes of the refractive index in the fluid. Interferometric methods visualize and measure phase shift distributions that can be integrated to give the absolute refractive index in the field of observation. For most fluids the refractive index can be converted into density by a simple relationship. The optical measurement of density distributions can be applied to totally different cases of moving or static fluid. In the field of gasdynamics the density changes due to dynamic effects. It is uniform throughout the gas when the gas is at rest. In free buoyant flows with heat transfer the density is a function of temperature only. When the heat transfer ceases the flow stops and the density gradients disappear. In stratified flows of incompressible fluids a positive density gradient in the direction of $\boldsymbol{g}$ exists already when the fluid is at rest and each fluid element sustains its density when set into motion.

In this work we consider a case of motion in a stratified liquid in which fluid elements represent harmonic oscillators swinging about their resting positions governed by the equilibrium of buoyant and inertia forces. At a fixed point of observation this motion causes a small harmonic disturbance of the stratification density since the fluid elements that pass the station originate from different heights. The observed disturbance is proportional to the element displacement times the stratification gradient in the direction of motion. At a neighbouring point of

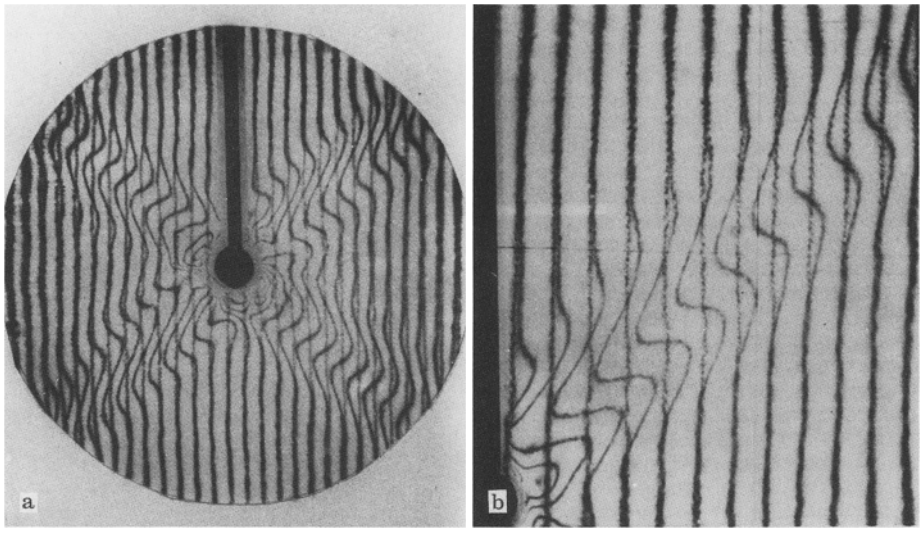

Fig. 1 a and b. **a** Superposition of interferograms without (straight fringes) and with cross wave. **b** Close-up of one beam of the cross wave

observation the harmonic disturbance might be shifted in phase. Then, there is a density gradient normal to the direction of motion and different from the stratification gradient. The interferometer with Wollaston prism applied in this work measures this gradient as function of space and time. Given the direction of motion this result converts directly into the gradient of displacement. A linear internal gravity wave is a continuum of such harmonic oscillators. For a special type, the so-called cross wave (Fig. 1 for illustration of the name), a theory is available (Thomas & Stevenson, 1972) that provides a full solution for the density disturbance as function of space and time. The present experiments serve to verify this theory.

The cross wave was first investigated by Görtler (1943) who already took some schlieren photographs. Later the subject was taken up again by Mowbray (1967) who employed shadow and schlieren techniques. Thomas and Stevenson (1972) measured local displacement amplitudes by means of a microscope, however, could not get measurements as function of time. Two interferometric investigations on stratified flows are known. Debler and Vest (1977) studied the feasibility of holographic interferometry in the case of horizontal stratified flow past a cylinder, and Stevenson et al. (1983) set up a six-mirror Mach-Zehnder interferometer to investigate the wave pattern behind a body moving at constant speed in a stratified liquid.

The type of flow in inner waves, i.e. oscillations of small amplitude and low frequency, does not allow the application of standard methods like pressure probes, hot wire or Laser-Doppler Anemometry. Interferometric methods are so far the only way to determine wave variables qualitatively in space and time. We believe that the present work is the first application of schlieren interferometry to stratified flows.

2 Theoretical background

We consider a liquid in which the density ϱ_0 is a function of y_0 only and require $\varrho_0(y_0)$ to satisfy

$$\omega_0^2 = -(g/\varrho_0)(d\varrho_0/dy_0) \tag{1}$$

for constant ω_0. When a two dimensional body having its long axis horizontal (a cylinder) is forced to oscillate laterally about its rest-position at a frequency $\omega < \omega_0$, a 2-dimensional wave pattern shaped like two crossing beams will occur (Fig. 1 a). Fluid motion is restricted to these beams fading away with distance from the body and from the centerline of the beams. The angle between the beams and the horizontal increases with ω.

We are dealing with a system in which a harmonically oscillating body force is acting on a non-isotropic (with respect to density gradient) liquid. Under isotropic conditions one would expect disturbances confined to a narrow region about the body. In the non-isotropic case disturbances can radiate away from the body as waves. The underlying effect is understood if the liquid is considered non-viscous. Then inertia and buoyancy can be balanced for a fluid element to let it swing like a mass-spring system at the natural frequency

$$\omega = \omega_0 \sin\theta \tag{2}$$

where θ is the angle between the direction of motion and the horizontal. The wave is then a continuum of such swinging fluid elements which has to satisfy conservation of mass and momentum under the boundary conditions observed in the experiment. The latter can only be fulfilled if viscous forces are respected. The theory of Thomas and Stevenson (1972) reveals that these forces are, however, of a lower order of magnitude than the dominant forces inertia and buoyancy. In this asymptotic sense Eq. (2) applies to the real (viscous) wave. This

means first that θ is equal to the angle between beam and horizontal and second that the direction of motion is predominantly parallel to the beams. The wave is a natural motion. To keep it up in a stationary state the secondary viscous forces are balanced by the pressure drop along the beam which again is balanced by the body force. Approaching the body along a beam the wave region of dominant inertia and buoyancy goes over into a transition zone where the pressure and viscous forces increase to the magnitude of the dominant forces and the natural motion of the wave turns into forced motion which is perfectly attained on the body's surface. The transition zone is made visible in Fig. 2.

Throughout this work we consider half a beam stretching upwards from the transition zone and fix coordinates as in Fig. 3. Every fluid element within the beam oscillates at the exciting frequency ω, i.e. at any point (x, y) the variables speed, density and pressure are proportional to $\exp(i\omega t)$. They are, however, phase shifted with respect to each other and each of them experiences a spatial change of phase. The theory of Thomas and Stevenson (1972) provides speed, density and pressure as functions of x, y and t. It is based on linearized equations, i.e. only small changes of the variables from the static values of the stratification are admitted. Similar to boundary layer theory the solution is obtained asymptotically for a small parameter ε in form of a similarity solution. The coordinate transformation (Fig. 3) is

$$\eta = \frac{1}{\varepsilon}\frac{(y/L)}{(x/L)^{1/3}} \tag{3}$$

with

$$\varepsilon = (2\,Re\cos\theta)^{-1/3} \tag{4}$$

defined by the Reynolds number and the angle θ. The angle θ is assumed not to come close to $\pi/2$ or zero so that small ε means high Re, which takes the form

$$Re = (g/\omega_0)\,L/\nu^* \tag{5}$$

with the characteristic length

$$L = g/\omega_0^2 . \tag{6}$$

We restrict to stratifications in which $y_0 \ll L$. Then the exponential function $\varrho_0(y_0)$ as required by Eq. (1) can be approximated by the linear function

$$\varrho_0 = \varrho^*(1 - y_0/L) \tag{7}$$

and the density disturbance ϱ can be written in the form

$$\varrho(x,y,t) = (a\varrho^*/\cos\theta)\,(x/L)^{-2/3} \cdot \{S_1(\eta)\cos(\omega t) + C_1(\eta)\sin(\omega t)\} . \tag{8}$$

The functions S and C are represented by integrals of the form

$$S_r = \int_0^\infty k^r \exp(-k^3)\sin(k\eta)\,dk \tag{9}$$

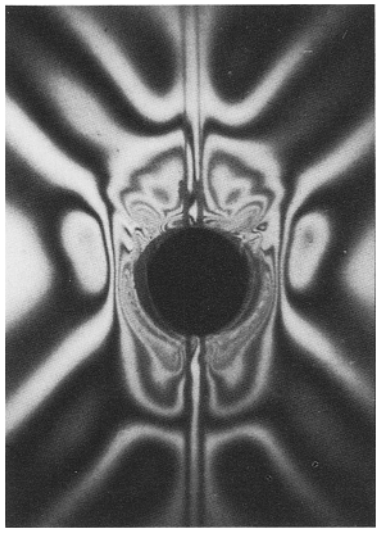

Fig. 2. Schlieren interferogram of cross wave with body and transition zone. The distance between the interference fringes is made infinite for this image

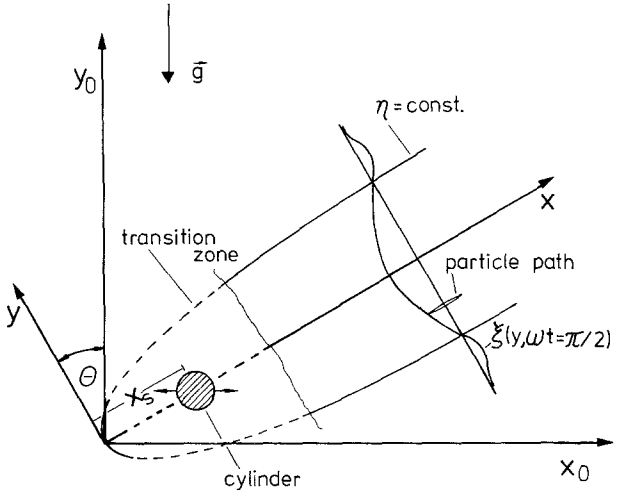

Fig. 3. Coordinate system

and

$$C_r = \int_0^\infty k^r \exp(-k^3)\cos(k\eta)\,dk\,, \quad r = 0, 1, 2, \ldots \tag{10}$$

with the following properties:

$$C_r(-\eta) = C_r(\eta)\,; \quad S_r(-\eta) = -S_r(\eta)\,, \tag{11}$$

$$\partial C_r/\partial\eta = -S_{r+1}\,; \quad \partial S_r/\partial\eta = C_{r+1}\,. \tag{12}$$

With these rules ϱ can be differentiated with respect to y. We get

$$\partial\varrho/\partial y = (a\varrho^*/\varepsilon\cos\theta)\,x^{-1} \cdot \{C_2(\eta)\cos(\omega t) - S_2(\eta)\sin(\omega t)\} . \tag{13}$$

Differentiation of ϱ with respect to x shows that $\partial\varrho/\partial x$ is of order 1 compared with order $1/\varepsilon$ for $\partial\varrho/\partial y$. For the experiments we will use therefore

$$\partial\varrho/\partial x_0 = -(\partial\varrho/\partial y)\sin\theta\,. \tag{14}$$

As already mentioned the fluid moves predominantly in x-direction. Therefore, the relationship between ϱ and the displacement ξ in x-direction is simply

$$\varrho = -\xi\,(d\varrho_0/dy_0)\sin\theta\,. \tag{15}$$

An example of $\xi(y)$ at a fixed time is indicated in Fig. 3.

3 Experiments

3.1 Properties and production of stratification

All experiments were conducted with brine in the density range 1.0 to 1.04 g/cm^3. For this range the density is proportional to the mass fraction m_s of the salt in the form

$$\varrho_0 = (0.7078\ \text{g/cm}^3)\,m_s + \varrho_{0w}\,. \tag{16}$$

The viscosity of brine was taken from Hodgman (1977). For the applied range at 20 °C it is approximately proportional to density. The kinematic viscosity ν was therefore considered constant and ν^* was set equal to $1.04\cdot10^{-6}$ m^2/s. The refractive index as function of density was measured by a Michelson interferometer and is plotted in Fig. 4. For the lower density range

$$n = 1.3322 + K(\varrho_0 - \varrho_{0w}) \tag{17}$$

applies with $\varrho_{0w}(20\,°\text{C}) = 0.9982$ g/cm^3 and $K = 0.248$ cm^3/g. An apparatus as sketched in Fig. 5 was developed for convenient production of stratifications. Basically two fluxes $\dot V_w$ (fresh water) and $\dot V_s$ (salt water) of different density are mixed by a calibrated double valve to give a constant flux $\dot V$ of varying density. $\dot V$ is about 5 cm^3/s allowing a small inlet velocity of about 1 mm/s through the manifold at the bottom of the tank. For the present experiments only uniform gradients [Eq. (7)] were produced up to 10^5 g/m^4. The produced gradients were checked by sampling at various heights of the tank.

3.2 Experimental set-up

Figure 6 depicts a top view of the principle set-up. A He-Ne-laser ($\lambda = 632.8$ nm) with beam expander serves as the coherent light source. Its plane of polarisation is adjusted to the Wollaston prism. The first mirror[1] makes a parallel beam of 243 mm diameter which enters the stratification tank normally. Front and rear wall are made from regular window glass framed to keep a distance of $l = 70$ mm between the panes. The waves are excited by a cylinder (Ø 20 mm) attached to a thin strut connected to a crank mechanism so as to swing about its center position at the desired frequency. The amplitude of the cylinder is smaller than its diameter. Behind the tank the light beam

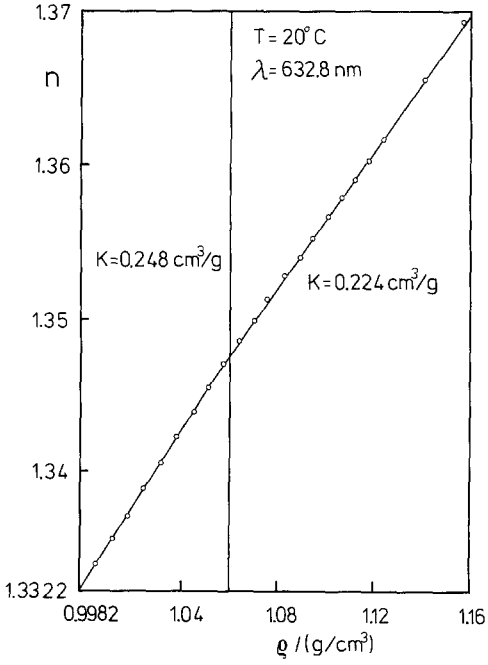

Fig. 4. Refractive index of brine as function of density measured by a Michelson interferometer

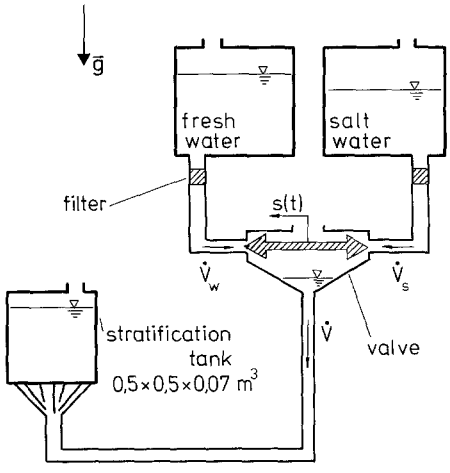

Fig. 5. Principle set-up of stratification apparatus

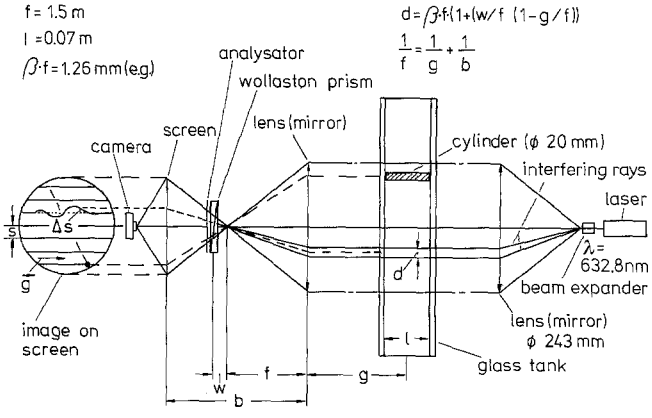

Fig. 6. Set-up of schlieren interferometer with Wollaston prism

is refocussed by a second mirror[1] a distance w before the Wollaston prism with analyser. The prism is oriented to generate straight vertical fringes in the case of no wave. The wave, producing density disturbances, causes the fringes to distort. The distorted fringe pattern can be photographed at a rate of three exposures per second. For illustration and evaluation both patterns, the disturbed and the undisturbed, can be superposed as shown in Fig. 1 b.

A few basic remarks on the Wollaston prism are necessary before going on with the present application. A more thorough analysis of the prism is found in Sernas (1977) or Merzkirch (1974). In the case of no density gradients in the fluid the Wollaston prism generates equidistant, straight interference fringes spaced at the distance

$$s = \frac{\lambda f}{\beta w} M. \tag{18}$$

β is a fixed prism angle and M is the image magnification on the screen. In case of density gradients the fringes are deformed and the relative displacement $\Delta s/s$ of any point on the fringe is given by

$$\frac{\Delta s}{s} = \frac{lK}{\lambda} \Delta \varrho . \tag{19}$$

$\Delta \varrho$ is the density difference between two points in the fluid separated by the distance

$$d = \beta f (1 + w/f (1 - g/f)) . \tag{20}$$

Their corresponding loci on the image lie $(M \cdot d/2)$ to either side of the deformed fringe while their connecting line stands normal to the undisturbed fringes. When $\Delta \varrho$ is small compared with the total range of ϱ (when d is sufficiently small) $\Delta \varrho/d$ can be approximated by $d\varrho/dz$ with z normal to the undisturbed fringes. In the present experiments the undisturbed fringes are oriented vertically. Therefore, there is no component of the stratification gradient normal to the fringes. The prism ignores the stratification gradient and we have

$$\frac{\partial \varrho}{\partial x_0} = \frac{\lambda}{l dK} \frac{\Delta s}{s} . \tag{21}$$

ϱ is already the density disturbance caused by the wave since $\partial \varrho_0/\partial x_0 = 0$.

Before applying this formula three associated problems ought to be discussed. In principle, it is possible to orient the undisturbed fringes at any angle with respect to the vertical. The prism always measures the density gradient normal to the undisturbed fringes. It would recognize the stratification as a disturbance and react with a constant shift $\Delta s/s$ of all fringes assumed the stratification gradient is uniform. The wave would then disturb this shifted pattern (however straight) and evaluation could be performed. The reason for selecting the vertical position of the undisturbed fringes is that small irregularities of the uniform stratification gradient do not appear in the undisturbed pattern.

For the evaluation of the interference fringes we assume that the light penetrates the stratification parallel to the layers. However, in reality the light is deflected due to the gradients of refractive index. A deflected ray experiences an additional phase shift because it passes layers of different refractive index. The deflection can be computed by evaluation of Fermat's principle (Merzkirch 1974). For gradients $\partial n/\partial z \ll n/l$ the ray displacement Δz at the exit of the tank can be approximated by

$$\Delta z = (l^2/2n) (\partial n/\partial z) . \tag{22}$$

$\partial n/\partial z$ is in the order of the stratification gradient, typically 0.02 m^{-1}. For $n = 1.3322$ and $l = 70$ mm we see that $\Delta z < 0.05$ mm. Since Δz again is much smaller than d (> 1 mm) the additional phase shift is negligible.

The use of the regular window glass for the tank raises the question if the thickness variation of the glass introduces an optical disturbance comparable to that being measured. A precision requirement is obtained from Eq. (19). The smallest detectable $\Delta s/s$ is about 0.05 (Merzkirch 1974). The product $(lK\Delta \varrho)$ is replaced by $2\Delta l n_{\text{glass}}$ where Δl is the thickness variation over the distance d. Then we have

$$\frac{2\Delta l}{d} < \frac{\lambda}{n_{\text{glass}}} 0.05 . \tag{23}$$

High quality window glass satisfies this requirement. It is, however, important to keep the glass walls parallel under water load otherwise the undisturbed fringes would not appear straight and equidistant.

3.3 *Evaluation procedures*

The basis for the comparison of theory and experiment are Eqs. (13, 14, 21) relating theoretical and experimental density gradients. The comparison could be carried out by integration of the experimental fringes for the explicit density disturbances ϱ. This is, however, disadvantageous because of inevitable large integration errors. Furthermore, the integration would not produce any more information than the direct comparison of the gradients which is applied here. Since $\Delta s/s$ is simply proportional to $\partial \varrho_0/\partial x_0$ we go on with $\Delta s/s$ and derive from Eqs. (13, 14, 21)

$$\frac{\Delta s}{s} (x, \eta, t) = - \phi_s (x) (C_2 (\eta) \cos (\omega t) - S_2 (\eta) \sin (\omega t)) \tag{24}$$

with

$$\phi_s (x) = \frac{l dK \varrho^* a \tan \theta}{\varepsilon \lambda} \frac{1}{x} . \tag{25}$$

1 Here for the sake of simplicity replaced by a lens

This equation provides $\Delta s/s$ in the entire flow field as function of time, however, it has yet to be decided which points $\Delta s/s(x, \eta, t)$ make up a fringe. The problem can best be solved by a computer program. In principle, a reference line $x_0 = \text{const}$ is chosen and $\Delta s/s$ is computed along a line $\eta = \text{const}$ until it fits the distance between the point of computation and the reference line. The procedure is repeated for as many lines $\eta = \text{const}$ as necessary to complete one fringe. The next fringe is then computed for $x_0 + s = \text{const}$ and so on. In Fig. 7 fringes successive in time are plotted for a fixed x_0. We note the following properties:

a) Any two fringes of phase shift π have identical zeros and their maxima lie on the same line $\eta = \text{const}$,

b) for $\omega t = 0; \pi$ the maxima coincide with $\eta = 0$ and zeros are found at $\eta_1 = \pm 1.77$ and $\eta_2 = \pm 5.48$,

c) for $\omega t = 3/2\pi; \pi$ zeros are found at $\eta = 0$ and $\eta_3 = \pm 3.57$.

We note that zeros are particularly well detectable making them convenient observables for use in evaluation.

From Eqs. (15, 21) we see that $\partial\xi/\partial y$ is equivalent to $\Delta s/s$. Because of the sine-like shape of a fringe its integral ξ has a similar shape and so the fringe is an indirect visualization of the particle displacement.

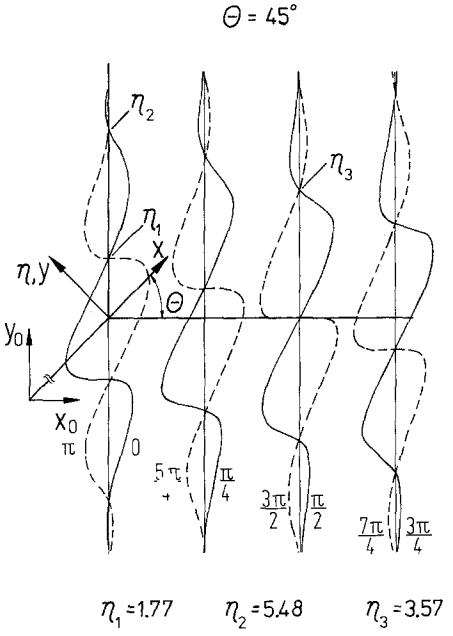

Fig. 7. Computed interference fringes for one period at a fixed x_0. For clarity fringes at different times are drawn side by side

4 Results

In the first place we study where the wave propagates. Equation (2) states that the beam of the cross wave and the horizontal form the angle θ. This is perfectly supported by Fig. 8. The angle θ is measured between the centerline of the beam ($\eta = 0$) and the horizontal. The similarity solution predicts the phase of $\Delta s/s$ [Eq. (24)] to stay constant on lines $\eta = \text{const}$ which spread with $x^{1/3}$ [Eq. (3)] while the amplitude attenuates with x^{-1}. The amplitude variation is meaningless for zero points $\Delta s = 0$ which are therefore suited to measure the spread of the wave. Figure 9 shows lines $\eta = \pm 1.77; \pm 3.57$ for $\theta = 30°$ and $\theta = 60°$. The lines correspond to $\Delta s = 0$ at $\omega t = 0; \pi$ and $\omega t = \pi/2; 3/2\pi$ respectively (Fig. 7). The width of the wave is greater for $\theta = 60°$ than for $\theta = 30°$. This is so because ε [Eq. (3)] depends on θ and thus y/L comes out greater for the greater angle. Experimental zero points obtained from the interferograms are plotted as circles for

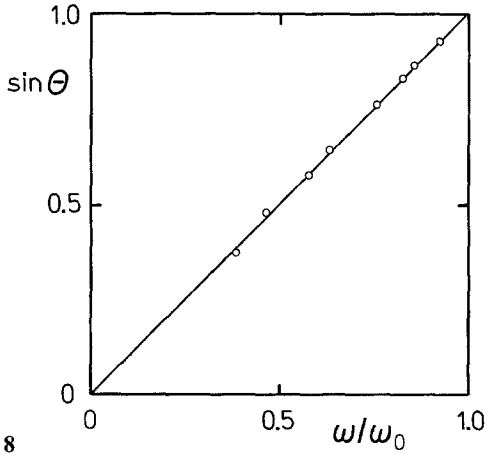

8

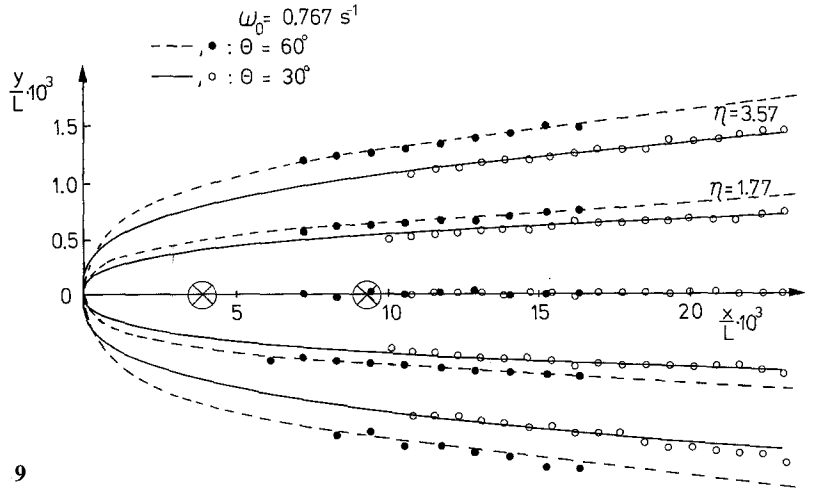

9

Figs. 8 and 9. **8** The angle θ measured against ω/ω_0 supporting Eq. (2); **9** The spread of the wave as predicted by the similarity curves $\eta = \text{const}$ and corresponding measurements of zero points ($\Delta s = 0$) of interference fringes. The big circles with cross indicate the location of the body. The left one pertains to $\theta = 60°$

$\theta = 30°$ and as dots for $\theta = 60°$. We see that the spread of the wave is perfectly confirmed.

However, this result involves two error sources which have to be pointed out. Neither a reference point in time nor the distance between the origin $x = 0$ and the body can be provided by experimental boundary conditions. This is an inherent feature of the linear theory which is confined to the natural wave motion independent of the body except for its frequency. Different bodies of the same frequency would produce identical waves. The waves require fictitious reference points in time and space which have to be localized in the actual interferograms by interpolation. The time problem can be solved by systematic comparison of successive fringe patterns with the theoretical patterns. This way a certain point of time can be discriminated to lie between two successive patterns. The symmetry properties of any two fringes which are half a period apart (see Fig. 7) are very useful for this procedure. The accuracy of the method depends on the number of patterns per period. Practically an error to a 1/50 of a period is achievable. The approach for the distance problem is the following. Knowing the zero point in time the points of Fig. 9 are plotted in the $x-y$ system starting at some arbitrary zero point for x. Then the $\eta-x$ system is shifted along x until Fig. 9 is obtained and thus the distance x_s/L is fixed. The criterion for the final position of the $\eta-x$ system ought to be a best possible fit of the points to the curves. Since the slope $d\eta/dx$ is small the determination of x_s is unsatisfactory. The error is in the order of $\Delta x/L = 10^{-3}$. The distance x_s depends on the amplitude A of the body under otherwise constant conditions. Figure 10 (solid symbols) shows for three different θ that x_s/L increases with growing amplitude. The explanation is that the transition zone grows with A and goes over into a wider wave requiring a greater x and x_s respectively. The limit of the body's amplitude is found to be

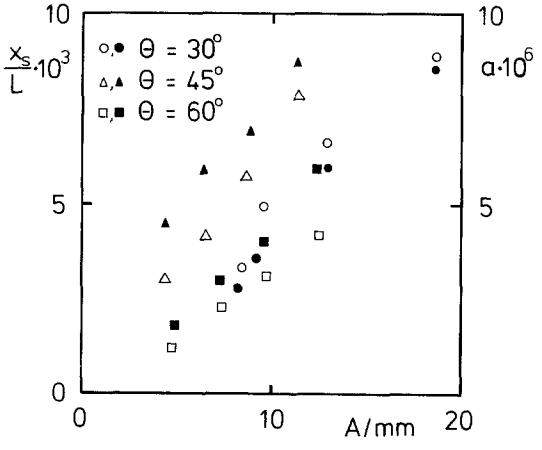

Fig. 10. The distance x_s as function of the body amplitude A (filled symbols) obtained from plots of which Fig. 9 is an example. The open symbols give $a(A)$ resulting from amplitude measurements like Fig. 12

about its diameter (20 mm). Above that other waves come into the picture and the similarity system is distorted.

A particular feature of the cross wave is that fluid velocity and phase velocity stand normal to each other (Lighthill 1978). The fluid moves parallel to x with no phase change while lines of constant phase ($\Delta s = 0$) move in negative y-direction as shown in Fig. 7. The phase velocity of the fringes is obtained from Eq. (24) when written in the form

$$\Delta s/s = \phi_s(x)\, E_2 \sin(\omega t - \arctan(C_2/S_2)) \tag{26}$$

where

$$E_2 = (S_2^2 + C_2^2)^{1/2} \tag{27}$$

is the envelope of the fringes, i.e. the maximum of $\Delta s/s$ at any η and x. Implicit differentiation of the phase $(\omega t - \arctan(C_2/S_2))$ using Eqs. (11, 12) gives the phase velocity as

$$\frac{\partial \eta}{\partial(\omega t)} = \frac{E_2}{S_2 S_3 + C_2 C_3} \tag{28}$$

which turns out to be practically constant for the experimental range of η. The distance-time relation appearing consequently as a straight line is compared in Fig. 11 with experimental results. Line and points represent zeros ($\Delta s = 0$) of the interference fringes which are precisely detectable. The predicted phase velocity is perfectly confirmed.

With Eq. (24) the theory predicts Δs to decay with $1/x$ along lines $\eta = \text{const}$ at fixed time. For experimental verification of this attenuation law we choose the maximum of Δs at $\omega t = 0$ and along $\eta = 0$. In Fig. 12 results for $\theta = 45°$ are displayed. The location of the points with respect to the body is determined like in Fig. 9. The curves correspond to Eq. (24). The free amplitude factor a is selected to allow for a best possible fit of curve and points. The four different sets of points correspond to different body amplitudes A. We see that the deviation from the $1/x$-law becomes evident with decreasing x and increasing A. In other words, the validity range of the linear theory is shifted away from the body with increasing A. The attenuation factor a being obviously dependent of A is plotted in Fig. 10 (open symbols) for three different angles θ. We find a to be roughly proportional to A for each θ. Among the angles 45° seems to be the most efficient for energy transfer from the body to the wave.

After having shown where the wave propagates, how it moves in time and how its amplitude attenuates Fig. 13 finally displays the development of a total experimental fringe over an entire period for one angle θ. The theoretical fringes correspond to those of Fig. 7. We see that the coincidence of theoretical and experimental fringes is excellent in the inner region of the wave, however, becomes worse towards the edge of the wave beam. Observations of successive periods show that these deviations do not repeat periodically. They rather fluctuate in an irregular

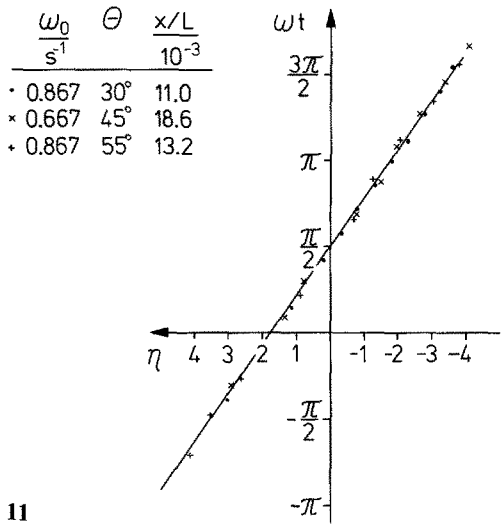

11

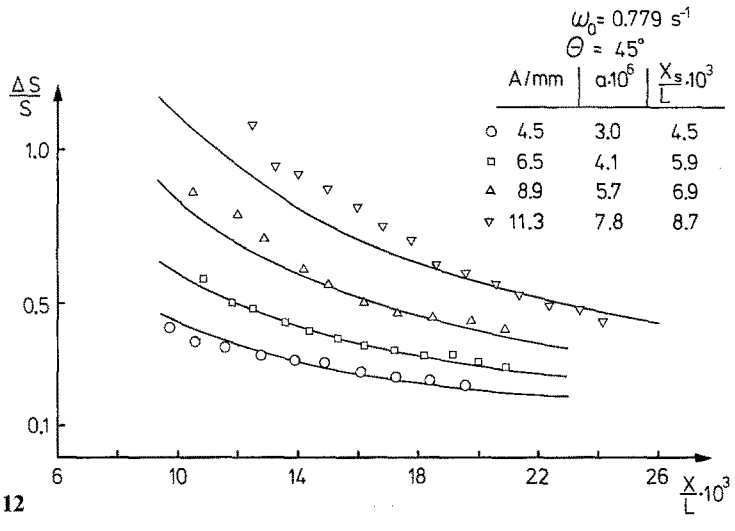

12

Figs. 11 and 12. 11 The distance-time relation as predicted for points $\Delta s = 0$ compared with measurements; **12** Amplitude attenuation displayed for $\theta = 45°$ and for different body amplitudes A. The curves give the a/x law of the linear (small amplitude) theory (Eq. (25)). Increasing deviation is found for decreasing x and growing A

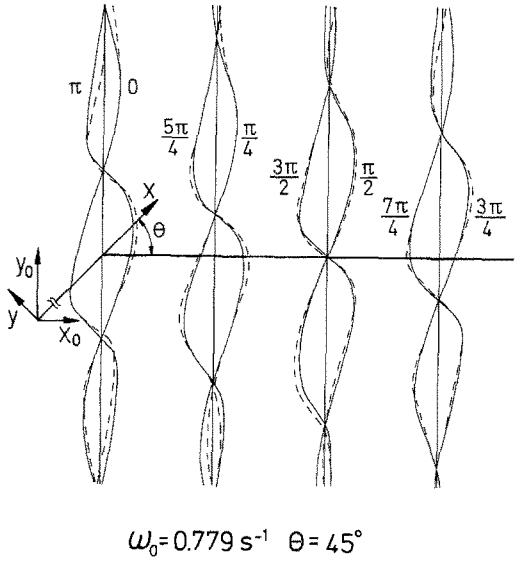

Fig. 13. An example of comparison of experimental (---) and theoretical fringes over an entire period

manner and seem to originate from weak reflections from the tank walls.

5 Conclusion

The schlieren interferometer with Wollaston prism is successfully applied to a wave motion in an incompressible fluid. The basis for this application is the stratification density gradient which is already there when the fluid is at rest. When set into motion the fluid elements sustain their static density and by moving relative to each other they produce density disturbances in other than the vertical direction. The gradients of these disturbances are detected by the interferometer. It is shown that sufficient information can be obtained from the interferograms to determine the propagation of an inner wave in space and time including amplitudes. The shape of the fringe profiles suggests to reduce the information mainly from the zero points and maxima which are precisely detectable. The displacement of the fringes is proportional to the density gradient of the disturbance which is analytically derived from the theory of the investigated cross wave (Thomas & Stevenson 1972). The theory, considering only small amplitudes, can in principle not provide the absolute amplitude and the relative position of body and wave in space and time. This requires interpolation giving rise to some experimental uncertainties. However, taking this into account the theory is extremely well supported by the experiments. The limit of the small amplitude approximation appears clearly in the amplitude attenuation measurement.

In conclusion, it can be said that the schlieren interferometer with Wollaston prism is a highly effective method for visualization and quantitative measurement of inner gravity waves. The range of the static gradient is limited by light deflection. An extension of the method to other types of stratified flow is conceivable.

Acknowledgements

The author wishes to thank Prof. W. Merzkirch who initiated and supported this work.

References

Debler, W. R.; Vest, C. M. 1977: Observation of a stratified flow by means of holographic interferometry. Proc. R. Soc. Lond. A. 358, 1–16

Görtler, H. 1943: Über eine Schwingungserscheinung in Flüssigkeiten mit stabiler Dichteschichtung. ZAMM 23, 2

Hodgman, C. 1977: Handbook of chemistry and physics. Cleveland: Chemical Rubber

Lighthill, I. 1978: Waves in fluids. London: Cambridge University Press

Merzkirch, W. 1974: Flow visualization. New York: Academic Press

Mowbray, D. E. 1967: A theoretical and experimental investigation of the phase configuration of internal waves of small amplitude in a density stratified liquid. J. Fluid Mech. 28, 1–16

Sernas, V. 1977: The Wollaston prism schlieren interferometer. Von Karman Institute Brussels, Lecture Series 96

Stevenson, T. N.; Woodhead, T. I.; Kanellopulos, D. 1983: Viscous effects in some internal waves. Appl. Sci. Res. 40, 185–197

Thomas, N. H.; Stevenson, T. N. 1972: A similarity solution for viscous internal waves. J. Fluid Mech. 54, 495–506

Received January 14, 1985

Announcements

Third international symposium on applications of laser anemometry to fluid mechanics, July 7 – 9, 1986, Lisbon, Portugal

The Symposium aims to present new results, of significance to fluid mechanics obtained by laser anemometry. It is intended that these results will improve present understanding of complex flows, both laminar and turbulent, and their implications for the solution of problems of fluid mechanics will be emphasised. Contributions to the theory and practice of laser anemometry will be presented where they facilitate new fluid-mechanic investigations.

Approximately 12 formal sessions and panel discussions are planned. Contributed papers are welcome in the following areas:

- jets, wakes and mixing regions,
- boundary layer flows,
- separated flows,
- particle sizing,
- reacting flows,
- flows with imposed oscillations,
- two phase flows,
- developments to optical and electronic instrumentation intended to improve accuracy and range of measurements.

Paper selection will be based upon a reviewed abstract of not less than 500 words which should be typed double spaced and state the purpose, results and conclusions of the work with supporting figures as appropriate. Five copies of the abstract should be submitted to: Professor D. F. G. Durão, Dept. of Mechanical Engineering, Instituto Superior Técnico, Avenida Rovisco Pais, 1096 Lisbon, Portugal.

Deadlines

December 13, 1985	Final date for receipt of abstracts
February 28, 1986	Author informed concerning acceptance
May 9, 1986	Final date for receipt of camera-ready manuscripts

All papers accepted for presentation will be incorporated in a Proceedings Volume which will be available at the time of the Symposium. It is intended that a bound volume subsequently be published and will contain a selection of extended papers.